Journal of Electron Spectroscopy and Related Phenomena 196 (2014) 43–48

Contents lists available at ScienceDirect

Journal of Electron Spectroscopy and Related Phenomena

journal homepage: www.elsevier.com/locate/elspec

New insight into dissociative photoionization of N_2O at ~20 eV using threshold photoelectron–photoion coincidence velocity imaging

Xiaofeng Tang[a,b], Xiaoguo Zhou[a,c,*], Binglin Qiu[a], Shilin Liu[a,c], Fuyi Liu[b], Xiaobin Shan[b], Liusi Sheng[b]

[a] Hefei National Laboratory for Physical Sciences at the Microscale, Department of Chemical Physics, University of Science and Technology of China, Hefei, Anhui 230026, PR China
[b] National Synchrotron Radiation Laboratory, University of Science and Technology of China, Hefei, Anhui 230029, PR China
[c] Synergetic Innovation Center of Quantum Information & Quantum Physics, University of Science and Technology of China, Hefei, Anhui 230026, PR China

ARTICLE INFO

Article history:
Available online 30 January 2014

Keywords:
Photoelectron–photoion coincidence
Velocity imaging
Dissociative photoionization
Synchrotron radiation
Nitrous oxide

ABSTRACT

Dissociative photoionization (DPI) of N_2O at ~20 eV has been reinvestigated with threshold photoelectron–photoion coincidence (TPEPICO) velocity imaging. In threshold photoelectron spectrum, a shoulder peak at 20.045 eV is observed close to the ground vibrational level of $C^2\Sigma^+$ state at 20.100 eV. Through comparing the coincident mass spectra recorded at 20.045 and 20.100 eV, the assignment of the shoulder band is corrected to a vibrational excited $D^2\Pi$ ionic state from the previous conclusions of the vibrationless level of $b^4\Pi$ or hot band of $C^2\Sigma^+$ state. For the dominant photofragment of NO^+ at 20.045 eV, TPEPICO time-sliced velocity image is measured to obtain the corresponding total kinetic energy and angular distributions. Interestingly, both the bimodal vibrational population and angular distribution of NO^+ fragment from dissociation of $N_2O^+(D^2\Pi)$ are very similar to those of $N_2O^+(C^2\Sigma^+)$ ions. With the aid of potential energy curves, the DPI mechanisms of N_2O via $D^2\Pi$ ionic state at 20.045 eV along the $NO^+(X^1\Sigma^+)+N(^2D)$ and $NO^+(X^1\Sigma^+)+N(^2P)$ dissociation channels are clarified, in which the internal conversion from $D^2\Pi$ to $B^2\Pi$ state is the rate-determined step.

1. Introduction

It is well-known that N_2O^+ molecular ion is a significant intermediate in an ion-molecule reaction, $O^+ + N_2 \rightarrow NO^+ + N$, which is one of the most important chemical processes in the upper ionosphere [1–3]. Therefore, numerous theoretical and experimental studies have been performed on its structure and dynamics. The neutral N_2O molecule has a valence electronic configuration of $(1\sigma)^2(2\sigma)^2(3\sigma)^2(4\sigma)^2(5\sigma)^2(6\sigma)^2(1\pi)^4(7\sigma)^2(2\pi)^4$. Once removing an electron from the outer orbitals, the low-lying $X^2\Pi$, $A^2\Sigma^+$, $B^2\Pi$ and $C^2\Sigma^+$ ionic states of N_2O^+ can be produced respectively. Moreover, a double electron excitation with the $(\ldots)(7\sigma)^2(2\pi)^2(3\pi)^1$ configuration can theoretically produce five ionic electronic states: one $^4\Pi$, one $^2\Phi$ and three $^2\Pi$, where the excitation energies of $^2\Pi$ and $^4\Pi$ ionic states are lower than that of $C^2\Sigma^+$ state.

Many spectroscopic techniques, e.g. He I photoelectron spectroscopy (PES) [4–6], threshold photoelectron spectroscopy (TPES) [7–9], pulsed field ionization photoelectron spectroscopy (PFI-PES) [10] and photofragment excitation (PHOFEX) spectroscopy [11] have been employed to investigate the molecular structure of ion and obtain the vibrational frequencies of electronically excited states. Additionally, dissociation of N_2O^+ at the low-lying electronic states has been explored by various experimental methods including electron impact ionization [12], photoionization mass spectrometry [13,14], fast-ion beam laser spectroscopy (FIBLAS) [15], PHOFEX velocity imaging [16,17], photoelectron–photoion coincidence (PEPICO) [18–20], threshold PEPICO (TPEPICO) [7–9,21] and vector correlation [22].

Based on these systemic investigations, dissociation mechanisms of the low-lying electronic states of N_2O^+ have been clarified, as well as kinetic and internal energy distributions of fragments. For $X^2\Pi$ state, many complex interactions, e.g. spin–orbit coupling, Fermi resonance, and Renner–Teller interaction associated with the v_2^+ bending excitation were revealed [10]. The first electronically excited state, $A^2\Sigma^+$, was found to decay via fluorescence and/or predissociation [7,18,20,21]. $NO^+(X^1\Sigma^+)$ ion and $N(^4S, ^2D)$ atom were its dissociation fragments, where a "channel switching" effect between the two dissociation limits, $NO^+(X^1\Sigma^+)+N(^4S)$ and $NO^+(X^1\Sigma^+)+N(^2D)$, was observed at the high vibronic levels [16]. Both the higher electronically states, $B^2\Pi$ and $C^2\Sigma^+$, were predissociative as well. A complex and unassigned spectral structure was observed for the $B^2\Pi$

* Corresponding author at: Hefei National Laboratory for Physical Sciences at the Microscale, Department of Chemical Physics, University of Science and Technology of China, Hefei, Anhui 230026, PR China. Tel.: +86 55163600031.
E-mail address: xzhou@ustc.edu.cn (X. Zhou).

0368-2048/$ – see front matter © 2014 Elsevier B.V. All rights reserved.
http://dx.doi.org/10.1016/j.elspec.2014.01.013

state as a long series of broad vibration-like peaks superimposed over a continuous background [10]. For dissociation of $B^2\Pi$ state, NO^+ and N_2^+ were the only detected fragments in which the abundance of N_2^+ was very small [7,20]. Moreover, the kinetic energy release distribution (KERD) of NO^+ was showed a bimodal structure, which corresponds to the $NO^+(X^1\Sigma^+)+N(^2D)$ and $NO^+(X^1\Sigma^+)+N(^2P)$ channels. [18–20] Within an excitation energy range of 19.9–20.7 eV, $N_2O^+(C^2\Sigma^+)$ ions were mainly produced. Through fast predissociation, four fragment ions, NO^+, N_2^+, O^+ and N^+ were observed in dissociation of $N_2O^+(C^2\Sigma^+)$, in which NO^+ and N^+ ions were dominant [7–9]. Recently, the kinetic and internal energy distributions of NO^+ fragments were measured directly after dissociation from a series of vibrational state-selected $N_2O^+(C^2\Sigma^+)$ ions [9]. A bimodal distributions were found in the KERD and corresponded respectively to the $NO^+(X^1\Sigma^+)+N(^2D)$ and $NO^+(X^1\Sigma^+)+N(^2P)$ channels as well as that case of $B^2\Pi$ state.

More interestingly, a shoulder vibronic band was observed at ~20 eV in the TPES [8,9], which was very close to the ground vibrational level of $C^2\Sigma^+$ state at 20.100 eV. It was definitely observed without assignment in the earlier zero kinetic-energy photoelectron spectrum [23], while it was not detected in high-resolution He I and He II photoelectron spectra [4–6,20]. Later, the band was tentatively identified as the vibrationless level of nearby *b* state in Chiang and Ma's TPES [8], according to that the shoulder band does not belong to a Rydberg series converging to $C^2\Sigma^+$ ionic state as shown in the previous photoionization efficiency curve [13]. However its excitation energy (~7.16 eV) was far from the theoretically predicted value (6.08 eV for $b^4\Pi$ state [24]). In addition, the $b^4\Pi$ assignment was unreasonable according to spin-forbidden transition from the neutral $N_2O(X^1\Sigma^+)$ molecule [25]. Based on energy interval between the detected vibronic levels of $C^2\Sigma^+$, the shoulder band at 20.045 eV was suggested to be the $1_0{}^1 2_3{}^0$ hot band of $C^2\Sigma^+$ by Chen et al. [10]. However, it is unusual that no other hot bands like $1_0{}^1 2_2{}^0$ and $1_0{}^1 2_1{}^0$ were observed. In the recent vector correlation experiments, it was still unassigned [22]. Therefore, the spectral assignment for the shoulder band at ~20 eV is still not clarified, and its dissociation mechanism is unknown as well.

Using the complete active space self-consistent field (CASSCF) and multireference configuration interaction (MRCI) methods, the electronic configurations and excitation energies of the low-lying electronic states of N_2O^+ were calculated [24]. An unreported lower electronic state, $D^2\Pi$ of N_2O^+ ion was theoretically expected near $C^2\Sigma^+$, whose vertical excitation energy was calculated as 6.95 eV at MRCI level of theory and even slightly lower than that of $C^2\Sigma^+$ (7.58 eV). Since its contour of potential energy surface, especially in the region of the lower vibronic levels, and equilibrium structure were similar to those of $B^2\Pi$ state, the v_2^+ bending mode was expected to be dominantly excited when $N_2O^+(D^2\Pi)$ ion was produced like $N_2O^+(B^2\Pi)$ ion [24]. The v_2^+ frequency is also expected close to that of $B^2\Pi$ state, 368 cm^{-1} [26]. Therefore, to find experimental evidence of the $D^2\Pi$ ionic state and its dissociation dynamics are the major aim of present study.

With the recently developed TPEPICO velocity imaging method [27], the dissociative photoionization (DPI) of N_2O at ~20 eV has been reinvestigated. A special attention is paid to comparison of the two DPI processes via the ground vibrational level of $C^2\Sigma^+$ state and the shoulder band at 20.045 eV. TPEPICO time-of-flight (TOF) mass spectra and the velocity distributions of NO^+ fragments are measured at the two excitation energies respectively. With the aid of the theoretical potential energy curves along the N–NO rupture coordinate, the shoulder band at ~20 eV in TPES is reassigned to a vibrational excited $D^2\Pi$ ionic state, and the corresponding DPI mechanism is finally proposed.

2. Experimental

Present TPEPICO experiments were performed at U14-A beamline of National Synchrotron Radiation Laboratory (Hefei, China). The detailed configurations of the beamline and TPEPICO velocity imaging spectrometer have been introduced previously [27–29], and thus only a brief description is presented here.

Synchrotron radiation emitted from an undulator was dispersed with a 6 m vacuum ultraviolet (VUV) monochromator equipped with a 370 grooves/mm spherical grating, which covers a photon energy range of 7.5–22.5 eV. In the present experiments, the widths of the entrance and exit slits of the monochromator were set at 80 μm, and thus the typical energy resolution power ($E/\Delta E$) was about 2000. A gas filter filled with neon was located behind the monochromator to eliminate higher-order-harmonic radiation. A silicon photodiode (International Radiation Detectors, SXUV-100) was installed to measure photon flux and normalize electron and ion signals.

A pure N_2O (99.9%) beam without further purification was expanded supersonically into vacuum chamber through a 30-μm-diameter stainless nozzle. The stagnation pressure is 1.1 atm. The molecular beam was collimated by a 0.5-mm-diameter skimmer and then crossed perpendicularly with synchrotron radiation in the extraction field of TPEPICO velocity imaging spectrometer. The typical backing pressures of source and ionization chambers of the spectrometer were 2×10^{-3} and 4×10^{-5} Pa respectively with the molecular beam on.

A double velocity imaging design was applied in the present TPEPICO spectrometer. Photoelectron and photoion were extracted simultaneously in opposite directions. Using a specially designed repelling electric field, the velocity map image of photoelectron was magnified and projected onto detector. A mask with a 1-mm-diameter hole and an outside concentric ring was located in front of the detector to collect threshold and energetic photoelectrons respectively. Due to a significant improvement on magnification of electron image, contamination of the most energetic electrons was suppressed in TPES and TPEPICO measurement [27]. In addition, a subtraction method [30] was further utilized to reduce the residual contamination of energetic electrons in TPES. The typical photoelectron energy resolution is ~9 meV. Using the detected threshold photoelectron as start signal for measuring the TOF of ion, the coincident ions were mapped by the focusing lens and projected onto a dual micro-channel plate (MCP, 40 mm diameter) backed by a phosphor screen (Burle Industries, P20). A thermoelectric-cooling charge couple device camera (Andor, DU934N-BV) was used to record image on the screen. By applying a pulsed high voltage on MCP as a mass gate, the target ions could be easily chosen to obtain its TPEPICO time-sliced velocity image.

3. Results and discussion

3.1. Threshold photoelectron spectrum of N_2O at ~20 eV

With an extraction electric field of 14 V/cm, TPES of N_2O in the excitation energy range of 19.9–20.5 eV was measured and shown in Fig. 1. Four main resonant peaks at 20.045, 20.100, 20.260 and 20.390 eV can be observed, and their corresponding energies and intensities agree very well with previous data [8,10]. As the previous investigation suggested [8,10], the three peaks at 20.100, 20.260 and 20.390 eV can be assigned as the (0,0,0), (1,0,0) and (0,0,1) vibrational bands of $C^2\Sigma^+$ state of N_2O^+, where the numbers in parentheses represent vibrational quanta for the v_1^+(symmetrical stretch), v_2^+(bending), and v_3^+(asymmetrical stretch) modes, respectively.

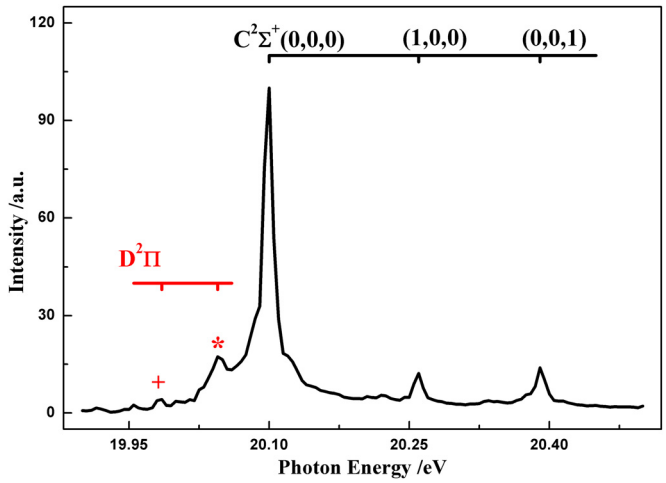

Fig. 1. Threshold photoelectron spectrum of N_2O in the excitation energy range of 19.9–20.5 eV.

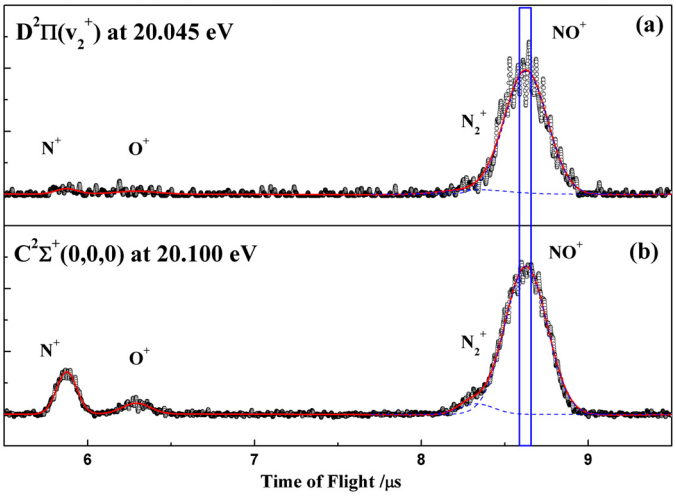

Fig. 2. TPEPICO TOF mass spectra for dissociation of N_2O^+ ions at 20.045 eV (a) and 20.100 eV (b), where the blue pane represents the mass gate of time-sliced coincident velocity imaging. (For interpretation of the references to color in this figure legend, the reader is referred to the web version of this article.)

Besides the three vibrational bands of $C^2\Sigma^+$ state, another shoulder peak at 20.045 eV can also be clearly discerned in the TPES and noted with a star in Fig. 1. As mentioned above, it was observed in the early zero kinetic-energy photoelectron spectrum [23], but undetected in high resolution He I and He II photoelectron spectra [4–6,20]. Later, the shoulder band was tentatively assigned to the vibrationless level of $b^4\Pi$ ionic state in Chiang and Ma's TPES [8], and reassigned as the $1_0{}^1 2_3{}^0$ hot band of $C^2\Sigma^+$ by Chen et al. [10]. Recently, it was suggested in the vector correlation experiments to be attributed to a weak vibrational band of $b^4\Pi$ or $D^2\Pi$ ionic states [22], both of which were lying in the Franck–Condon gap between the $B^2\Pi$ and $C^2\Sigma^+$ states. Unfortunately, more detailed discussion and dissociation mechanism were absent.

Both $D^2\Pi$ and $b^4\Pi$ states are the double excited electronic states with the electronic configuration of $(1\sigma)^2\ldots(1\pi)^4(7\sigma)^2(2\pi)^2(3\pi)^1$ [25]. As calculated by Chambaud et al. [24], vertical excitation energies of the $C^2\Sigma^+$ and $D^2\Pi$ ionic states are 7.58 eV and 6.95 eV at MRCI level, while that of $b^4\Pi$ state is 6.08 eV. Thus within the present excitation energy range, $D^2\Pi$ and/or $b^4\Pi$ ionic states probably contribute the shoulder band in TPES. However, the photoionization transition of $N_2O^+(b^4\Pi) \leftarrow N_2O(X^1\Sigma^+)$ is spin-forbidden [25], and hence the $b^4\Pi$ assignment is unreliable. Another possible assignment of the $1_0{}^1 2_3{}^0$ hot band of $C^2\Sigma^+$ state suggested by Chen et al. [10] is unreasonable too, because no other hot bands were observed in experiments and the shoulder band did not belong to a Rydberg series converging to $C^2\Sigma^+$ ionic state in the previous photoionization efficiency curve [13]. Therefore it is most likely contributed from a bending excitation band with a few $v_2{}^+$ quanta of the $D^2\Pi$ state, since its shape of potential energy surface and equilibrium structure are similar to those of $B^2\Pi$ state. [25]. In addition, there is another weak peak located at the lower energy than that of the shoulder band in TPES of Fig. 1, which is noted with a cross. Its excitation energy is 19.985 eV, and the energy interval between the "cross"-noted and the "star"-noted peaks is 0.06 eV (484 cm^{-1}). According to energy uncertainty of the present experiment (~9 meV), the interval is reasonably close to the $v_2{}^+$ frequency of $B^2\Pi$. Unfortunately, the "cross"-noted peak is too weak to perform measurements of the coincident TOF mass spectrum and velocity image. In the following sections, the shoulder band is noted as the $D^2\Pi(v_2{}^+)$ state for convenient description.

3.2. TPEPICO time-of-flight mass spectra

Fixed the photon energy at 20.045 and 20.100 eV respectively, TPEPICO TOF mass spectra from $D^2\Pi(v_2{}^+)$ and $C^2\Sigma^+(0,0,0)$ levels were measured and presented in Fig. 2. No N_2O^+ parent ions was detected in the mass spectra, indicating that the $D^2\Pi(v_2{}^+)$ state is also completely dissociative. Although two excitation energies are very close, the dissociation fragments were different from $D^2\Pi(v_2{}^+)$ and $C^2\Sigma^+(0,0,0)$ states. For dissociation of $D^2\Pi(v_2{}^+)$ state, only NO^+ and $N_2{}^+$ fragments can be discerned and the abundances of O^+ and N^+ fragments are almost negligible. Interestingly, the fragmentation of $N_2O^+(D^2\Pi)$ ions is very similar to that of lower $B^2\Pi$ ionic state [7,20] and far different from the nearby $C^2\Sigma^+$ state [8,9,20], in which the $N_2O^+(C^2\Sigma^+)$ ions can dissociate and produce all the $N_2{}^+$, NO^+, O^+, and N^+ fragments. Thus the present coincident TOF mass spectra provide additional evidence of our new assignment at 20.045 eV that the shoulder band is confessedly not contributed from the hot band of $C^2\Sigma^+$ state.

As shown in Fig. 2, NO^+ fragments is the most predominant for dissociation of N_2O^+ in both $D^2\Pi(v_2{}^+)$ and $C^2\Sigma^+(0,0,0)$ level. The TOF profiles of NO^+ fragments at 20.045 and 20.100 eV are remarkably broadened due to the released kinetic energy in dissociation. Thus the time-sliced velocity images of NO^+ at two excitation energies are expected to reveal their dissociation mechanism.

3.3. TPEPICO time-sliced velocity image of NO^+ fragment

Several previous experimental investigations have been performed to measure the KERD in dissociation of N_2O^+ at ~20 eV. Through fitting TOF profile of fragments, an average kinetic energy released in the dissociation of N_2O^+ ions along the N–NO rupture at 20.045 eV was calculated to be 1.44 eV [8]. In the vector correlation measurement [22], the rough total KERD in dissociation of N_2O^+ ions at the shoulder band was extended up to ~3 eV with the maximum distribution at 1.3 eV. However, the detailed kinetic energy distribution in DPI of N_2O at ~20 eV was unrevealed due to the limited energy resolution of the previous studies.

As shown in our recent investigations of a few small molecules [9,31–35], the KERD in dissociation can be accurately acquired from the TPEPICO velocity map images. The corresponding resolution power, $\Delta E/E$, of kinetic energy distribution is as good as 3% [27]. Moreover, the angular distribution of fragment ions can be further obtained from the detected image. Thus more dynamic details are expected to be obtained by applying the novel TPEPICO velocity imaging method to DPI process of N_2O at ~20 eV. As shown in Fig. 2, the TOF profiles of NO^+ dissociated from N_2O^+ ion in both $D^2\Pi(v_2{}^+)$ and $C^2\Sigma^+(0,0,0)$ levels are significantly broadened to about 700 ns

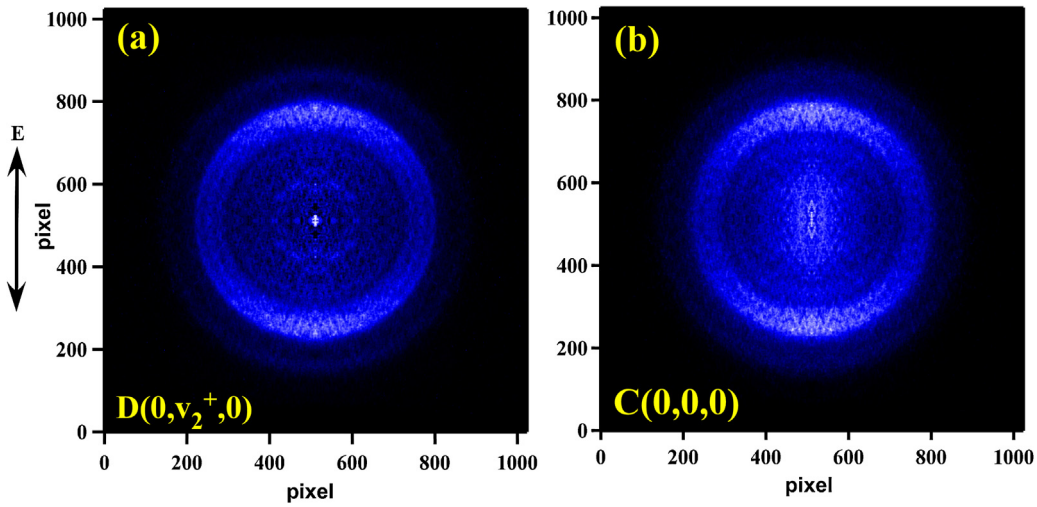

Fig. 3. TPEPICO time-sliced velocity images of NO^+ fragments dissociated from N_2O^+ ions in $D^2\Pi(v_2^+)$ state at 20.045 eV (a) and in $C^2\Sigma^+(0,0,0)$ state at 20.100 eV (b).

of full width. Thus TPEPICO time-sliced velocity images of NO^+ are obtained with a mass gate of 80 ns and presented in Fig. 3, where the electric vector ε of VUV photon is along vertical direction. Both images in Fig. 3 exhibit very similar structures, where two main concentric rings can be discerned. It means that NO^+ fragments have a typical bimodal distribution as dissociation of $B^2\Pi$ and $C^2\Sigma^+$ states. The bright inner ring is of the higher intensity than the outer one, and both diameters of two rings are very close in both images of Fig. 3. Moreover, both the images in Fig. 3 exhibit a tendency of slight parallel distribution along the electric field vector of photon.

By accumulating the intensity of image over angle, speed distribution of NO^+ fragments can be acquired. Based on the conservation of linear momentum in dissociation, the total KERD can be obtained subsequently. Fig. 4 displays the total KERDs in dissociation of N_2O^+ at $D^2\Pi(v_2^+)$ and $C^2\Sigma^+(0,0,0)$ states. Benefiting from the high energy resolution of present TPEPICO velocity imaging, more detailed structures are exhibited than that of the previous investigations [8,22]. Corresponding to the two concentric rings of image, the total KERD curves in Fig. 4 also show the bimodal distributions. The lower kinetic energy distribution has a large abundance with a center at 1.4 eV, which agrees with the previous conclusions [8,22]. The higher energy distribution is mostly populated at ~2.6 eV for dissociation of N_2O^+ at both $D^2\Pi(v_2^+)$ or $C^2\Sigma^+(0,0,0)$ states.

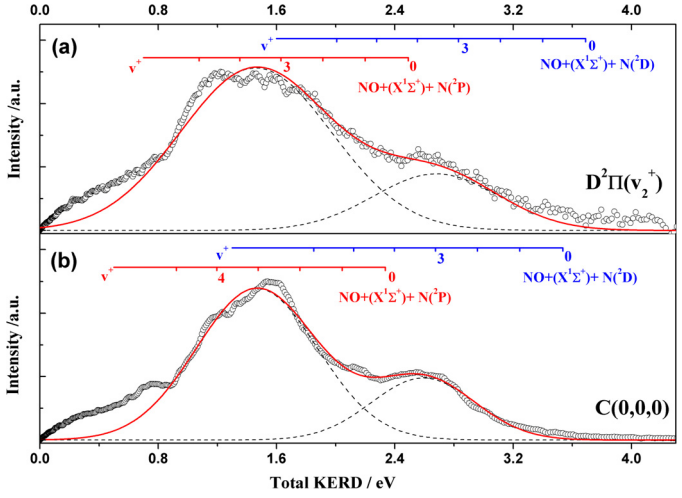

Fig. 4. Total kinetic energy release distributions in dissociation of N_2O^+ ions in $D^2\Pi(v_2^+)$ (a) and $C^2\Sigma^+(0,0,0)$ states (b).

Based on the energy conservation in dissociation, the internal energy E_{int} of NO^+ and the total released kinetic energy E_T have the following relation,

$$h\nu - D_0 = E_{avail} = E_{int} + E_T \quad (1)$$

where $h\nu$ is the excitation photon energy, D_0 is the dissociation limit for a specific channel, and E_{avail} is the available energy after dissociation. At the present excitation energy, three NO^+ formation pathways are energetically accessible: $NO^+(X^1\Sigma^+)+N(^4S)$ at 14.19 eV, $NO^+(X^1\Sigma^+)+N(^2D)$ at 16.57 eV and $NO^+(X^1\Sigma^+)+N(^2P)$ at 17.77 eV. Taking into account the vibrational frequency v^+, 2376.42 cm^{-1} [36] and an anharmonic parameter $\omega_e\chi_e$, 16.262 cm^{-1} of $NO^+(X^1\Sigma^+)$ ion [37], the vibrational state distributions of NO^+ fragment dissociated from N_2O^+ ion at $D^2\Pi(v_2^+)$ and $C^2\Sigma^+(0,0,0)$ states can be calculated.

For DPI process of N_2O at 20.045 eV, the total KERD is extended to 3.8 eV as shown in Fig. 4(a), and thus NO^+ fragmentation along the lowest dissociation channel $NO^+(X^1\Sigma^+)+N(^4S)$ is negligible. Due to the large energy difference between the two dissociation limits of $NO^+(X^1\Sigma^+)+N(^2D)$ and $NO^+(X^1\Sigma^+)+N(^2P)$, it is straightforward to attribute the lower kinetic energy distribution to contribution of the $NO^+(X^1\Sigma^+)+N(^2P)$ dissociation path, while the higher kinetic energy part is from the $NO^+(X^1\Sigma^+)+N(^2D)$ channel. The vibrational distribution of $NO^+(X^1\Sigma^+,v^+)$ extends from $v^+=0$ to 6 with a maximum intensity at $v^+=4$ for both dissociation channels as shown in Fig. 4. Both the distributions show very similar quasi-Gaussian profiles as the same as those in Fig. 4(b), and exhibit vibrational population reversion. In summary, the internal and kinetic energy distributions of NO^+ fragment dissociated from N_2O^+ in $D^2\Pi(v_2^+)$ state are almost the same as those of $C^2\Sigma^+(0,0,0)$ state.

From Fig. 3(a), angular distribution of NO^+ fragments can be derived from integrating the image over a proper range of speed at each angle. Subsequently, the anisotropic parameters β for different dissociation pathways can be calculated by fitting the angular distribution. For dissociation of N_2O^+ in $D^2\Pi(v_2^+)$ state at 20.045 eV, the anisotropic parameters β along the $NO^+(X^1\Sigma^+)+N(^2D)$ and $NO^+(X^1\Sigma^+)+N(^2P)$ pathways are 0.75 and 0.60 respectively, while those are 0.64 and 0.56 for dissociation of N_2O^+ in $C^2\Sigma^+(0,0,0)$ state [9]. These slightly more positive β values indicate that the $D^2\Pi(v_2^+)$ state has slightly more rapid dissociative rate than $C^2\Sigma^+(0,0,0)$. The β value observed in the previous (V_{NO+}, V_e, P) vector correlation experiment was 0.5 at 20.9 eV [38], which is consistent with our present data according to uncertainty measurement.

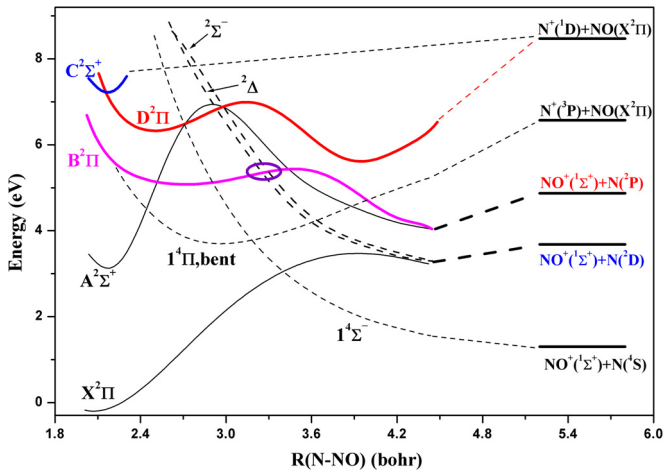

Fig. 5. Adiabatic correlation diagram for the low-lying electronic states of N_2O^+ ions along N–NO rupture coordinate.

3.4. Predissociation mechanism of N_2O^+ in $D^2\Pi$ state at 20.045 eV

As mentioned above, the coincident TOF mass spectra indicate that the shoulder band at 20.045 eV should be attributed to the vibrational band of $D^2\Pi$ ionic state, and it could rapidly predissociate along N–NO^+ rupture coordinate as well as the nearby $B^2\Pi$ and $C^2\Sigma^+$ electronic states. However, its fragmentation to produce N^+ atomic ion is far different from the nearby $C^2\Sigma^+$ state. The energy distributions of NO^+ fragment dissociated from N_2O^+ in $D^2\Pi(v_2^+)$ and $C^2\Sigma^+(0,0,0)$ states are almost the same as shown in the KERDs. Thus the dissociation mechanism of N_2O^+ in $D^2\Pi(v_2^+)$ state along the N–NO^+ rupture pathway is similar to that of $N_2O^+(C^2\Sigma^+)$ ions. With the aid of theoretical potential energy curves of N_2O^+ ion along the N–NO rupture coordinate, the DPI mechanism of N_2O at ~20 eV to produce NO^+ fragments can be inferred.

The molecular structures and excitation energies of low-lying electronic states of N_2O^+ ion were calculated by Chambaud et al. [24]. Fig. 5 shows a schematic diagram of their potential energy curves along N–NO coordinate, which are plotted with the reading points of the enlarged copy of the published figures. The lowest dissociation limit $NO^+(X^1\Sigma^+)+N(^4S)$ adiabatically correlates with $1^4\Sigma^-$ dissociative state. The $X^2\Pi$ ground state, together with $^2\Sigma^-$ and $^2\Delta$ repulsive states, correlates adiabatically to the second dissociation limit, $NO^+(X^1\Sigma^+)+N(^2D)$. Both the $A^2\Sigma^+$ and $B^2\Pi$ excited states link adiabatically with the $NO^+(X^1\Sigma^+)+N(^2P)$ dissociation limit, but $A^2\Sigma^+$ state is linear and $B^2\Pi$ is bent. The adiabatically dissociation products of $D^2\Pi$ and $C^2\Sigma^+$ states are $N^+(^1D)$ and $NO(X^2\Pi)$, whose dissociation limit is far higher than present excitation energy. In addition, the $D^2\Pi$ state is also bent with a similar shape of potential energy curve to that of $B^2\Pi$ state, especially in the region of the lower vibronic levels. Therefore, the v_2^+ bending mode of $N_2O^+(D^2\Pi)$ ions should be excited in the Franck–Condon region during photoionization.

Since the total KERD and anisotropic parameters in dissociation of $N_2O^+(D^2\Pi,v_2^+)$ ion along NO^+ formation pathway are very similar to those of $C^2\Sigma^+(0,0,0)$ state [9], the corresponding dissociation mechanisms are probably the same. Therefore, the NO^+ formation from dissociation of $N_2O^+(D^2\Pi,v_2^+)$ ion is suggested as the following.

The internal conversion from $D^2\Pi$ state to the lower $B^2\Pi$ state is the most critical step in overall dissociative photoionization process, as the same as observed in dissociation of $N_2O^+(C^2\Sigma^+)$ ion [9]. Then the $B^2\Pi$ state can directly dissociate to produce $NO^+(X^1\Sigma^+)$ and $N(^2P)$ fragments along its adiabatic potential energy surface. On the other hand, the coupling between the $B^2\Pi$ state and $^2\Sigma^-$ (or $^2\Delta$) repulsive states can also cause N_2O^+ ion to dissociate to $NO^+(X^1\Sigma^+)$ and $N(^2D)$ fragments.

Since both $D^2\Pi$ and $B^2\Pi$ states are bent, it is easier to couple with $B^2\Pi$ state than the linear $C^2\Sigma^+$ state in the Franck–Condon region. Thus the internal conversion from $D^2\Pi(v_2^+)$ to $B^2\Pi$ is more favorable than it from $C^2\Sigma^+$ state. Because the rate-determining step of overall dissociation processes of N_2O^+ ions is the internal conversion to $B^2\Pi$, the dissociation rate from $N_2O^+(D^2\Pi)$ ions is slightly faster than that of $N_2O^+(C^2\Sigma^+)$ ion. The prediction is also consistent with the present conclusion derived from the β measurements.

Additionally, only the $N^+(^3P)+NO(X^2\Pi)$ channel is energetically accessible for the N^+–NO rupture of both $D^2\Pi$ and $C^2\Sigma^+$ states in the present energy range. As shown in Fig. 5, the N^+ formation mechanisms of two states are expected totally different due to their different symmetries and potential energy surfaces. A probable explanation for the $N^+(^3P)$ formation pathway of $C^2\Sigma^+$ state is via internal conversion to the $A^2\Sigma^+$ state followed by spin–orbit coupling to $1^4\Pi$ state and then adiabatic dissociation. Obviously, the pathway is negligible for $D^2\Pi$ state due to competition along the NO^+ production channel. Of course, it remains to be an intriguing open question and is still needed to perform further investigation.

4. Conclusion

Using the novel method of TPEPICO velocity imaging, DPI of N_2O at ~20 eV has been reinvestigated. In threshold photoelectron spectrum, a shoulder peak at 20.045 eV is observed and close to the ground vibrational level of $C^2\Sigma^+$ state at 20.100 eV. However, the fragment ions dissociated from N_2O^+ ions at these bands are apparently different. At 20.100 eV, all the thermodynamic allowed fragment ions, N_2^+, NO^+, O^+, and N^+ are detected, while only NO^+ and a very small abundance of N_2^+ fragments are observed at 20.045 eV. Thus the assignment of the shoulder band at 20.045 eV is corrected to a vibrational excited $D^2\Pi$ ionic state from the previous conclusions of the vibrationless level of $b^4\Pi$ or hot band of $C^2\Sigma^+$ state.

For the dominant fragment of NO^+, TPEPICO time-sliced velocity images are measured at 20.045 and 20.100 eV to obtain the total kinetic energy distributions and anisotropic parameters. The almost same bimodal vibrational distributions are observed in the two total KERDs, which correspond to the $NO^+(X^1\Sigma^+)+N(^2D)$ and $NO^+(X^1\Sigma^+)+N(^2P)$ dissociation channels. The anisotropic parameters of dissociation of $N_2O^+(D^2\Pi)$ and $N_2O^+(C^2\Sigma^+)$ ions are very similar as well. With the aid of potential energy curves of low-lying electronic states of N_2O^+ along the N–NO rupture coordinate, both the $NO^+(X^1\Sigma^+)+N(^2D)$ and $NO^+(X^1\Sigma^+)+N(^2P)$ dissociation mechanisms of DPI at 20.045 eV are suggested. The internal conversion from $D^2\Pi$ to $B^2\Pi$ state is rate-determined step for both pathways. Then $N(^2P)$ can be produced from adiabatic dissociation of $B^2\Pi$ state, while the coupling between the $B^2\Pi$ state and $^2\Sigma^-$ (or $^2\Delta$) repulsive states cause N_2O^+ ion to dissociate to $NO^+(X^1\Sigma^+)$ and $N(^2D)$ fragments.

$$N_2O \underset{\rightarrow}{h\nu} N_2O^+(D^2\prod, v_2^+) \underset{\rightarrow}{IC} N_2O^+(B^2\prod) \begin{cases} \xrightarrow{\text{direct disso.}} NO^+(X^1\sum^+) + N\ (^2P) \\ \rightarrow {}^2\sum^-/{}^2\Delta < / \rightarrow NO^+(X^1\sum^+) + N(^2D) \end{cases} \quad (2)$$

Acknowledgments

This work is financially supported by the National Natural Science Foundation of China (NSFC, Grant nos. 21373194, 21073173, 21027005 and 21303177) and National Key Basic research Special Foundation (NKBRSF, Grant nos. 2013CB834602 and 2010CB923300).

References

[1] D.G. Hopper, J. Am. Chem. Soc. 100 (1978) 1019, and references therein.
[2] J.W. Duff, D.R. Smith, J. Atmos. Sol.-Terr. Phys. 62 (2000) 1199.
[3] X. Li, Y.L. Huang, G.D. Flesch, C.Y. Ng, J. Chem. Phys. 106 (1997) 1373.
[4] M.J. Weiss, Chem. Phys. Lett. 39 (1976) 250.
[5] P.M. Dehmer, J.L. Dehmer, W.A. Chupka, J. Chem. Phys. 73 (1980) 126.
[6] C.R. Brundle, D.W. Turner, Int. J. Mass Spectrom. Ion Phys. 2 (1969) 195.
[7] I. Nenner, P.M. Guyon, T. Baer, T.R. Govers, J. Chem. Phys. 72 (1980) 6587.
[8] S.Y. Chiang, C.I. Ma, J. Phys. Chem. A 104 (2000) 1991.
[9] X.F. Tang, M.L. Niu, X.G. Zhou, S.L. Liu, F.Y. Liu, X.B. Shan, L.S. Sheng, J. Chem. Phys. 134 (2011) 054312.
[10] W.W. Chen, J.B. Liu, C.Y. Ng, J. Phys. Chem. A 107 (2003) 8086.
[11] H.F. Xu, Y. Guo, Q.F. Li, S.L. Liu, X.X. Ma, J. Liang, H.Y. Li, J. Chem. Phys. 119 (2003) 11609.
[12] J.L. Olivier, R. Locht, J. Momigny, Chem. Phys. 68 (1982) 201.
[13] J. Berkowitz, J.H.D. Eland, J. Chem. Phys. 67 (1977) 2740.
[14] T. Masuoka, S. Mitani, J. Chem. Phys. 90 (1989) 2651.
[15] S. Abed, M. Broyer, M. Carre, M.L. Gaillard, M. Larzilliere, Chem. Phys. 74 (1983) 97.
[16] H.F. Xu, Y. Guo, Q.F. Li, Y. Shi, S.L. Liu, X.X. Ma, J. Chem. Phys. 121 (2004) 3069.
[17] H. Wang, X.G. Zhou, S.L. Liu, B. Jiang, D.X. Dai, X.M. Yang, J. Chem. Phys. 132 (2010) 224309.
[18] J.H.D. Eland, Int. J. Mass Spectrom. Ion Phys. 12 (1973) 389.
[19] B. Brehm, R. Frey, A. Kustler, J.H.D. Eland, Int. J. Mass Spectrom. Ion Phys. 13 (1974) 251.
[20] E. Kinmond, J.H.D. Eland, L. Karlsson, Int. J. Mass Spectrom. 187 (1999) 437.
[21] M. Richardviard, O. Atabek, O. Dutuit, P.M. Guyon, J. Chem. Phys. 93 (1990) 8881.
[22] M. Lebech, J.C. Houver, D. Dowek, R.R. Lucchese, J. Chem. Phys. 120 (2004) 8226.
[23] R. Locht, G. Hagenow, K. Hottmann, H. Baumgartel, Chem. Phys. 151 (1991) 137.
[24] G. Chambaud, H. Gritli, P. Rosmus, H.J. Werner, P.J. Knowles, Mol. Phys. 98 (2000) 1793.
[25] J.C. Lorquet, C. Cadet, Int. J. Mass Spectrom. Ion Phys. 7 (1971) 245.
[26] T. Cvitas, L. Klasinc, B. Kovac, R. McDiarmid, J. Chem. Phys. 79 (1983) 1565.
[27] X.F. Tang, X.G. Zhou, M.L. Niu, S.L. Liu, J.D. Sun, X.B. Shan, F.Y. Liu, L.S. Sheng, Rev. Sci. Instrum. 80 (2009) 113101.
[28] L. Gong, W.Z. Fang, F.Y. Liu, X.B. Shan, L.S. Sheng, Z.Y. Wang, J. Electron Spectrosc. Relat. Phenom. 182 (2010) 134.
[29] W.Z. Fang, L. Gong, X.B. Shan, F.Y. Liu, Z.Y. Wang, L.S. Sheng, J. Electron Spectrosc. Relat. Phenom. 184 (2011) 129.
[30] B. Sztaray, T. Baer, Rev. Sci. Instrum. 74 (2003) 3763.
[31] X.F. Tang, X.G. Zhou, M.L. Niu, S.L. Liu, L.S. Sheng, J. Phys. Chem. A 115 (2011) 6339.
[32] X.F. Tang, X.G. Zhou, M.M. Wu, Y. Cai, S.L. Liu, L.S. Sheng, J. Phys. Chem. A 116 (2012) 9459.
[33] X.F. Tang, X.G. Zhou, M.M. Wu, S.L. Liu, F.Y. Liu, X.B. Shan, L.S. Sheng, J. Chem. Phys. 136 (2012) 034304.
[34] X.F. Tang, X.G. Zhou, M.M. Wu, Z. Gao, S.L. Liu, F.Y. Liu, X.B. Shan, L.S. Sheng, J. Chem. Phys. 138 (2013) 094306.
[35] X.F. Tang, X.G. Zhou, Z.F. Sun, S.L. Liu, F.Y. Liu, L.S. Sheng, B. Yan, J. Chem. Phys. 140 (2014) 044312.
[36] J.E. Bartmess, in: P.J. Linstrom, W.G. Mallard (Eds.), NIST Chemistry WebBook, NIST, Gaithersburg, 2005.
[37] J.A. Coxon, M.A.A. Clyne, D.W. Setser, Chem. Phys. 7 (1975) 255.
[38] M. Lebech, J.C. Houver, D. Dowek, R.R. Lucchese, J. Chem. Phys. 117 (2002) 9248.